Barrier Jets during TAMEX[1]

Yi-Leng Chen, Jun Li and Hsi-Chyi Yeh

Department of Meteorology, University of Hawaii, Honolulu, HI 96822

Abstract

A barrier jet is frequently found along the northwestern coast of Taiwan in the prefrontal southwesterly flow regime during TAMEX. It has a maximum wind speed ($\geq$ 14 m s^{-1}) around 1 km above the surface with a vertical wind shear ~ 10 m s^{-1} × 10^{-3} s^{-1} below and ~ 4 m s^{-1} × 10^{-3} s^{-1} above. The horizontal scale of the barrier jet is on the order of 10^2 km.

During TAMEX, the southwesterly monsoon flow strengthens over the Taiwan area when the low-level pressure trough/surface front moves toward the southeastern China coast. The barrier jet occurs under the prefrontal southwesterly flow regime. It is a result of the airflow over the island obstacle under a low Froude number (0.2 - 0.5) flow regime. During the occurrence of a barrier jet, a windward pressure ridge is observed along the western coast due to blocking of the prevailing low-level flow by the island obstacle. Below the average height of the central mountain range, the incoming southwesterly flow decelerates off the southwestern coast and moves around the island. Along the western coast, the deflected airflow accelerates northward with a large cross-contour wind component down the pressure gradient along the northwestern coast, resulting in a barrier jet there. The barrier jet reaches the maximum intensity when the surface windward ridge/lee-side trough pressure pattern is most significant. It dissipates after a surface front arrives over northwestern Taiwan.

1. Introduction

Strong winds or jet streams in the lower troposphere have generated considerable interest because of their importance to air-pollutant transport, thunderstorm development, wind energy production, and aviation safety. A strong low-level flow near and parallel to a mountain range is generally referred to as a barrier jet (Schwerdtfeger 1975; Parish 1982; Overland and Bond 1993). The barrier jet is often associated with a cold-air damming on the slope of a mountain range and is caused by a strong low-level pressure-gradient force perpendicular to the mountain ranges due to the local enhanced baroclinity (Bell and Bosart 1988; Doyle and Warner 1991). It is also noted that some of the strong low-level winds near and parallel to coastal mountains is neither associated with the cold-air damming nor with locally enhanced low-level temperature gradients between the ocean and the land (Overland 1984). Overland and Bond (1995) suggested that this type of barrier jet only depends on the strength and the stability of the upstream flow, and the scales (height, width, and length) of mountain ranges. Lack of detailed observations on the interaction between the low-level prevailing flow and coastal mountain ranges has limited our understanding about this type of strong barrier winds.

Two-thirds of island Taiwan is mountainous. The central mountain range is oriented in the NNE-SSW direction with an averaged terrain height of about 2 km and the mountain peak exceeding 3.8 km (Fig. 1). During the early summer rainy season (May-June) over Taiwan, the southwest monsoon flow prevails in the low levels. Both the dynamic blocking of the low-level airflow and the thermally induced local circulations are significant (Wang 1986; Kuo and Chen 1990). The Taiwan Area Mesoscale Experiment (TAMEX) provides a unique opportunity to study the blocking of the low-level flow by the island topography (Kuo and Chen 1990). Based on several TAMEX case studies (i.e., Chen and Li 1995a,b; Li et al. 1996), we define the barrier jet as a strong southwesterly flow along the northwestern coast if the low-level flow accelerates down the pressure gradient along the northwestern coast and the along-shore wind component (V_s) has a maximum value ($\geq$ 10 m s^{-1}) between 0.5 and 1.5 km over northwestern Taiwan. In this study, we will survey

all the barrier jet events during TAMEX and examine the general characteristics of the jets in terms of their structure, horizontal extent and evolution. During the occurrences of the barrier jet, we will also investigate the relationship between upstream, low-level flow conditions, which are related to the synoptic-scale flow pattern, and local pressure patterns over the Taiwan area, which are induced by the orographic blocking of the prevailing flow, during the occurrences of the barrier jets. In addition, the role of the barrier jets in the enhancement of rainfall over northwestern Taiwan will be discussed.

2. Data sources

The low-level wind data were mainly obtained from routine upper-air soundings over East Asia and the high-resolution TAMEX soundings (totally 10 stations, Fig. 1) (Cunning 1988). In this study, high-resolution wind data at four sounding stations (station 46695, 46685, 46751 and ship station RCHY, Fig.1) over the northwestern Taiwan area are used to identify the barrier jet and to estimate its horizontal scale. The aircraft data are also used to analyze the spatial structure of the barrier jet. In addition, radar data at three Doppler radar stations along the northwestern coast are also used in our analysis.

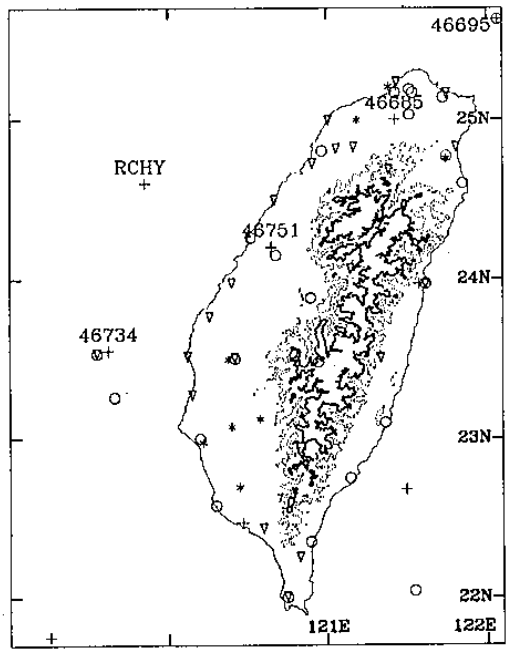

Figure 1 Location of sounding stations (+), the Central Weather Bureau (CWB) surface stations (o) and tower stations (▽). The terrain contours are 0.0 (solid), 1.0 (dashed) and 2.0 (heavy solid) km, respectively.

During TAMEX, the surface data were obtained from 74 surface observation stations and 21 wind tower stations (Cunning 1988). Wind speed, wind direction and temperature were recorded at most surface stations every hour, increasing to every half-hour during IOPs (Cunning 1988). The Central Weather Bureau (CWB) stations (total 25 stations, Fig. 1) recorded routine three-hour data (wind speed and direction, pressure, temperature, and dew-point) throughout the entire experiment (Chen and Schumann 1990). For tower stations (Fig. 1), the wind speed and direction were measured every 10 min at a height of ~ 10 m above the ground.

3. General characteristics of barrier jets along the northwestern coast during TAMEX

a. Vertical distribution

Figure 2a shows the time series of the along-shore wind component (V_s), averaged in the layer 0.5 - 1.5 km, at station 46685 (25.0°N, 121.4°E, Fig. 1) during TAMEX. The averaged V_s-component was greater than 10 m s^{-1} at 0600 UTC 13 May, 1200 UTC 16 May, 1800 UTC 21 May, 0000 UTC 22 May, 1200 UTC 22 May, 0000 UTC 27 May, 0000 UTC 2 June, 0000 UTC 7 June, 0000 UTC 22 June, 1200 UTC 22 June, 0000 UTC 23 June, 0600 UTC 23 June, 0000 UTC 24 June, and 1200 UTC 24 June, respectively (Fig. 2a). For all these times, the wind profiles at this station showed strong southwesterly winds with a maximum V_s-component greater than 10 m s^{-1} at ~ 1 km. Thus, there were seven barrier jet events (13-14 May, 16 - 17 May, 21 - 22 May, 26 - 27 May, 1 - 2 June, 7 - 8 June, and 22 - 25 June) during TAMEX.

The averaged profile of the V_s-component for the above observational times shows a maximum V_s-components of ~ 14 m s^{-1} at ~ 1 km (Fig. 3a). The vertical shear is about 10×10^{-3} s^{-1} below the level of the jet core (~ 1 km) and ~ 4×10^{-3} s^{-1} above, respectively. The standard deviations of the V_s-components at 1 km is ~ 5 m s^{-1} (Fig. 3a), indicating a large variation in the strength of barrier jets from case to case. The averaged profile of virtual potential temperature (θ_V) for the above observational times exhibits a small change with respect to the height in the lowest 1 km (Fig. 3b). The θ_V changes rapidly in the layer of 1.0 - 1.3 km and continues to increase with

height above the layer. The vertical profile of virtual potential temperature indicates that the depth of the mixing boundary layer is about 1 km (Stull 1988). The alongshore wind maximum (the barrier jet) occurs at the top (~ 1 km) of the mixing boundary layer along the northwestern coast.

b. Horizontal features

Chen and Li (1995a) analyzed the low-level airflow and pressure patterns over the Taiwan area for the 21-22 May (IOP 3) case. They showed that a windward ridge/lee-side trough sea level pressure pattern developed over the Taiwan area when the strong southwesterly flow upstream of Taiwan had a large angle impinging on the central mountain range as a low-level pressure trough/surface front moved toward the southeastern China coast (Fig. 4a). The horizontal distribution of the D-value deviations at the 900-m level also exhibited a windward pressure ridge.

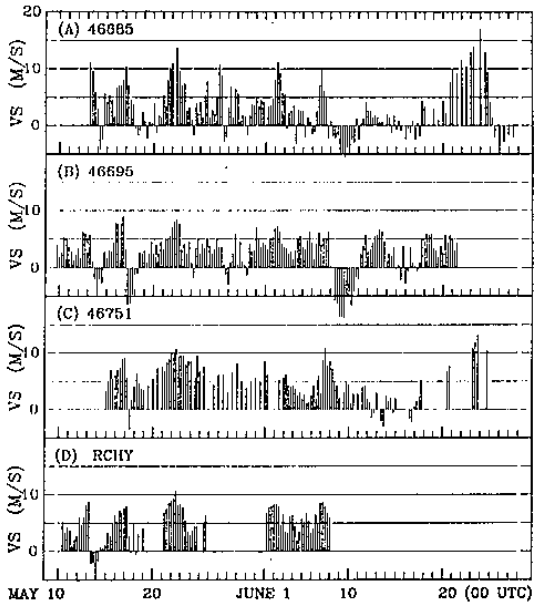

Figure 2 (a) Time series of the V_s-component, averaged in the layer 0.5 - 1.5 km, for station 46685 (a), 46695 (b), 46751 (c), and RCHY (d).

It was caused by adiabatic cooling as the incoming flow experienced forced ascent. The lee-side trough is a result of adiabatic warming on the lee side when the airflow aloft moved across the central mountain range (Smith 1979, 1982; Sun et al. 1991; Lin et al 1992). At the 900-m level, the flow deceleration was evident off the southwestern coast (Fig. 4b) as the southwesterly flow encountered high pressure there. The low-level airflow split off the southwestern coast and moved around the island, consistent with the theoretical studies of the airflow over an isolated island for a low-Froude-number ($F_r \leq 0.5$) flow regime (e.g., Smolarkiewicz et al. 1988; Sun et al. 1991). Along the western coast, the low-level airflow at the 900-m level was almost parallel to the coast line. It had a cross-contour wind component down the windward pressure ridge and

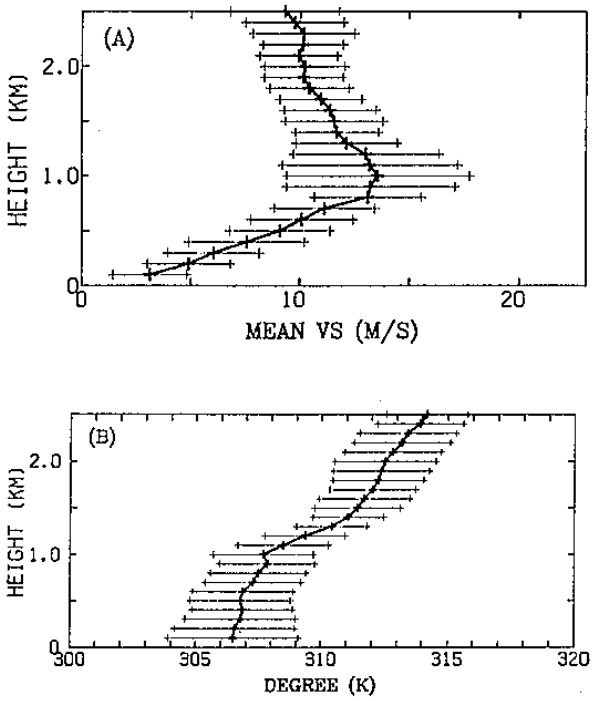

Figure 3 (a) The mean vertical profile (heavy line) of the V_s-component and the standard deviations (+) computed from the data for the 14 observational times. (b) Same as in (a) except for virtual potential temperature.

accelerated downstream (Figs. 4b). A barrier jet with a maximum wind speed greater than 15 m s^{-1} was observed along the northwestern coast (Fig. 4b). The wind speed reduced significantly to 10 m s^{-1} immediately north of the island. Above 2 km, the average height of the central mountain range, the flow acceleration along the west-northwestern coast was not significant (Chen and Li 1995b).

To further investigate the flow acceleration along the northwestern coast, a simple estimation of the acceleration, the pressure gradient force and the Coriolis force is made from the aircraft data at two flight levels (900 m and 2500 m) along the flight

tracks between point A (23°N) and B (25°N) (Fig. 4.b). For a coordinate system along the northwestern coast,

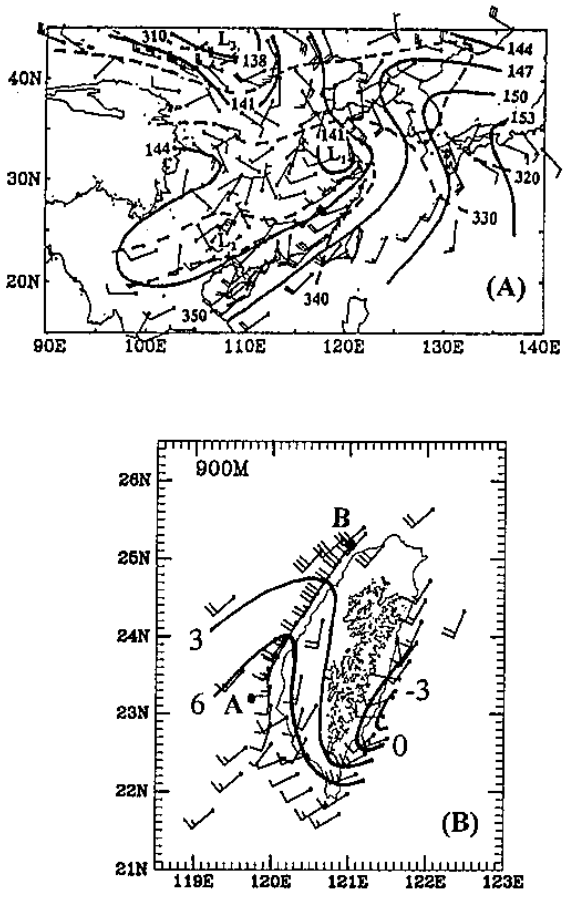

Figure 4 (a) Synoptic-scale chart at 850 hPa for 1200 UTC 21 May 1987. (b) Winds and deviations of D-value from the areal mean at the 900-m level around 1500 UTC 21 May. Geopotential heights in (a) every 30 m; deviations of D-value every 3 m. Winds (m s^{-1}) with one pennant, full barb and half barb represent 25, 5 and 2.5 m s^{-1}, respectively. The horizontal wind field in (b) is constructed from rawinsonde, pibal, and aircraft data during 1330-1720 UTC 21 May 1987 (After Chen and Li, 1995b).

tracks between point A (23°N) and B (25°N) (Fig. 4.b). For a coordinate system along the northwestern coast, the equation of motion for the V_s wind component can be written as

$$\frac{Dv_s}{Dt} = -\frac{\partial \Phi}{\partial s} - fV_n + F_R \qquad (1)$$

I II III

where terms I to III and F_R represent the acceleration, the pressure gradient force, the Coriolis force and the frictional force, respectively. The pressure gradient force is calculated from the D-value along the flight tracks. The Coriolis parameter is 5.9×10^{-5} s^{-1}.Under steady state assumption, term I at the 900-m level can be simply estimated by V_s ($\Delta V_s/\Delta S$), where ΔS is the distance between point A and B, V_s is the mean wind speed, and ΔV_s is the difference of the wind speed between A and B. It is found that at the 900-m level, the acceleration and the pressure gradient force are the dominant terms in equation (1) (Table 1), The result suggests that the flow accelerating downstream along the northwestern coast is mainly caused by the pressure gradient. Note that the local change term ($\partial V_s/\partial t$) can affect the estimated magnitude of the term I in Table 1 because the barrier jet was developing during the flight period (Chen and Li 1995b). At the 2500-m level, the along-shore pressure gradient force is nearly balanced by the Coriolis force in the along-shore direction, and the flow acceleration is quite small as compared to either the pressure gradient or the Coriolis

Flight Level / Parameters	900 m	2500 m
V_n (m s^{-1})	0.8	5.5
V_s (m s^{-1})	9.5	11.0
ΔV_s (m s^{-1})	8.1	2.0
$\Delta \Phi$ (m)	6.7	7.1
term I (10^{-4} m s^{-2})	2.4	1.3
term II (10^{-4} m s^{-2})	3.2	4.1
term III (10^{-4} m s^{-2})	-0.5	-3.3
Residual (10^{-4} m s^{-2})	-0.3	0.5

Table 1 One-dimensional estimation of the force balance along the flight tracks between A and B (Fig. 4b) at the 900-m and 2500-m levels. Δ and overbar represent a horizontal difference between A and B along the flight tracks and an averaged value within the range, respectively. Terms I to III and the residual term in equation (1) are calculated from aircraft data at these two levels between A and B.

force (Table 1). At this time, a low-level pressure system (L_1) was located to the north of the island (Fig. 4a). The pressure gradients at the 2500-m level are related to synoptic-scale low-level pressure patterns. These results suggest that above the average height of the central mountain range (~ 2 km), the large-scale flow and pressure pattern are not affected by the island mountains significantly.

To determine the horizontal extent of the barrier jets, we compare the averaged V_s-component in the layer 0.5 - 1.5 km among four sounding stations (station 46685, 46695, 46751 and RCHY) over the northwestern Taiwan area. For the seven barrier jet cases, the V_s-component at station 46685 always had the largest values among these four stations (Figs. 2), consistent with the aircraft observations (Fig. 4b). Station 46695 (25.0°N, 121.4°E) is located about 110 km northeast of station 46685 (Fig.1). The averaged V_s-component at station 46695 was always less than 10 m s^{-1} (Fig. 2a). For the seven barrier jet cases, the averaged ratio of the V_s-component at station 46695 to that at station 46685 was about 52%, indicating that barrier jets weaken considerably after moving away from the island. At station 46751 (25.0°N, 121.4°E), about 120 km south-southwest of station 46685, the averaged V_s-component for three barrier jet cases (21 - 22 May, 7 - 8 June and 22 - 25 June) was greater than 10 m s^{-1}. For the seven barrier jet cases, the averaged ratio of the V_s-components between station 46751 and 46685 was about 63%. These results suggest that the along-shore length scale of the barrier jet is approximately 200 km or less, consistent with the aircraft observations for IOP 3 (Fig. 4b).

The width of the barrier jet is difficult to determine from TAMEX data because there is only one sounding station (RCHY, 25.0°N, 121.4°E) in the direction normal to the jet axis (Fig.1). In addition, the sounding observations at this station only covered five barrier jet cases (13 -14 May, 16 - 17 May, 21 - 22 May, 26 - 27 May, 1 - 2 June, and 7 - 8 June) during TAMEX(Fig. 2d). For these five cases (totally 8 observational times), the V_s-component at station RCHY was less than 10 m s^{-1} during TAMEX except at 1200 UTC 22 May. The averaged ratio of the V_s-component between station RCHY and 46685 for these five cases was about 61%. The ship station, RCHY, is about 90 km west of the northwestern coast (Fig. 1). The distance may be comparable to the offshore length scale of the jet.

Theoretical analysis indicates that for the coastal mountain area under a small Froude number flow regime (Fr < 1), the disturbance will grow seaward to a horizontal distance given by a Rossby radius L_R (Overland and Bond, 1995):

$$L_R = (NH_s/f) = V/f \qquad (\text{if } Fr < 1) \qquad (2)$$

where N and H_s are the Brünt-Väsälä frequency, and the gravity height scale (Smith 1989), respectively. For the TAMEX barrier jet cases, V is about 5 - 10 m s^{-1}. Thus, the Rossby radius L_R is about 80 - 160 km, which is consistent with the offshore length scale of the barrier jet estimated from our observational data.

c. Evolution

The principal component (PC) analysis shows three dominant modes for the sea-level pressure patterns and two dominant modes for the surface winds over the Taiwan area during TAMEX (Chen and Li 1995a). Based on the timing of the maxima/minima in the PC scores of these dominant modes for eight episodes of the surface frontal passage during TAMEX, Chen and Li (1995a) classified the general evolution of surface airflow and sea-level pressure patterns over the Taiwan area in response to the low-level flow change during a frontal passage into 6 stages (totaly ~ 3 days). From stage 1 to 2, a windward ridge develops along the southwestern coast with a lee-side trough along the eastern coast with the intensification of the low-level southwesterly flow (Fig. 5a). The windward pressure ridge reaches the maximum intensity at stage 2. The vertical profile of the along-shore wind component (V_s) at station 46685 shows that the barrier jet develops between stages 1 and 2 (Fig. 5d). The maximum V_s-component occurs around 1 km in vertical and its magnitude reaches the maximum (~ 14 m s^{-1}) at stage 2 (Fig. 5d) when the sea-level windward ridge/lee-side trough pressure pattern is most significant. At stage 2, the significant increase of the V_s-component at the 1-km level is consistent with the strong pressure gradient along the northwestern coast at this stage (Chen and Li 1995a).

The barrier jet begins to weaken (Fig. 5d) as the surface front arrives over northwestern Taiwan (Chen and Li 1995a). As found in the IOP 13 case, the barrier jet was present in the prefrontal region along the northwestern coast (Li et al 1996). After stage 3, the barrier jet disappears (Fig. 5d) because of arrival of the surface front over the island. The shallow, northeasterly flow prevails in the postfrontal region over the island

(Chen and Li 1995a).

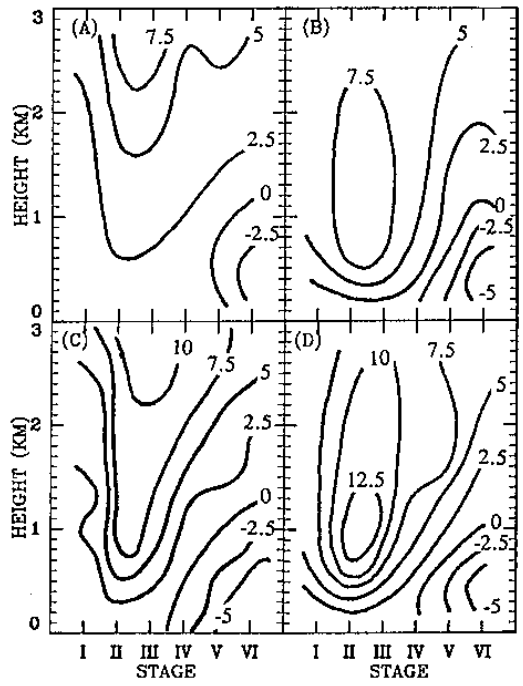

Figure 5 The height-time (stage) sections for the composite rawinsonde wind components (every 2.5 m s^{-1}): (a) and (b) for the wind component normal to the central mountain range (V_n) and parallel to the mountain range (V_s) at station 46734 (23.55°N, 119.62°E, Fig. 1), respectively. © and (d) same as in (a) - (b) except for station 46685 (25.00°N, 121.40°E, Fig. 1).

4. Upstream conditions for barrier jet events

To examine the characteristics of the upstream flow for the barrier jet events, we analyze following parameters for the upstream low-level southwesterly flow during TAMEX: wind speed, wind direction, atmospheric stability (i.e., N), and Fr. For the southwesterly flow regime, N is about 1.1 - 1.7 × 10 s^{-1} during TAMEX (not shown). The variation of the Froude number is mainly related to the intensity of the wind speed of southwesterly flow. The barrier jet occurred along the northwestern coast when the upstream Fr is in the range 0.3 -0.5 (not shown). As shown in Figure 4a, the upstream southwesterly flow intensifies when a low-level trough approaches the southeastern China coast. Figure 7 shows the synoptic-scale winds and geopotential height patterns at the 850-hPa level for the remaining five barrier jet cases during TAMEX. It is apparent that during TAMEX all barrier jets occurs when the 850-hPa trough moves toward the southeastern China coast with a strong southwesterly flow upstream of Taiwan as found by Chen and Li (1995b) for the IOP 3 case.

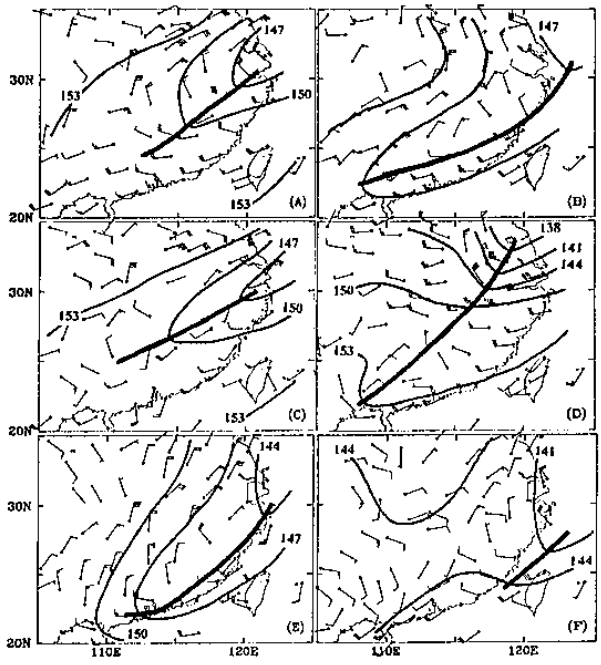

Figure 6 Synoptic maps at the 850-hPa level for (a) 0000 UTC 13 May, (b) 1200 UTC 16 May, (c) 0000 UTC 27 May, (d) 0000 UTC 2 June, (e) 0000 UTC 7 June and (f) 1200 UTC 24 June. Geopotential heights and winds plotting conventions same as in Fig. 4.

5. Role of the barrier jet in the enhancement of rainfall over northwestern Taiwan

a. Case of IOP 13

During 24-25 June, heavy rainfall occurred over northwestern Taiwan with the maximum (≥ 231 mm/day) along the northwestern coast. Li et al (1996) showed that the heavy rain was caused by a long-lived, convective rainband in the prefrontal atmosphere. It occurred in an upper-level divergence region and along the axis of the maximum equivalent potential temperature at the 850-hPa level. Because the hilly terrain along the southeastern China coast retarded the cold air behind a surface front, a low-level wind-shift line associated with a 850-hPa pressure trough moved toward northwestern Taiwan over the Taiwan Strait

before the arrival of the surface front. As the low-level wind-shift line approached the northwestern coast, the westerly flow coming from the southeastern China coast behind the trough interacted with the barrier jet along the Taiwan northwestern coast to form a strong, localized low-level convergence zone (~ 3 km deep). A long-lived rainband develops in the low-level convergence zone and produced heavy precipitation along the northwestern coast. The most intense convection associated with the wind-shift line occurred in the prefrontal atmosphere.

Li et al. (1996) also found that there were several long-lived (> 2 hr) reflectivity maxima embedded in the rainband. Figure 9 show a schematic diagram of the mesoscale airflow in the storm environment and the evolution of the long-lived reflectivity maxima embedded in the rainband. The reflectivity maxima formed on the southwestern tip of the rainband and along the low-level wind-shift line associated with the pressure trough. These reflectivity maxima often had several individual cells with much shorter life time. At the early stage of the reflectivity maxima, upward motion was observed over the low-level wind-shift line. During their movement from the southwest to the northeast along the rainband, these maxima intensified within the convergence zone where the barrier jet interacted with the westerlies behind the wind-shift line. At the well-developed stage, radar echoes associated with the reflectivity maxima extended to high levels and leaned vertically forward (southeastward) in the middle and upper levels because the hydrometeors were advected southeastward by the northwesterly flow aloft. In addition to the low-level inflow from the front (southeast), the westerly flow also entered the storm from the rear and converged with the ascending air entering from the front. The low-level convergence zone extended upward and tilted northwestward with height. The strongest ascending motion occurred over the low-level convergence zone and was collocated with the reflectivity maximum. Upward motion was observed in the anvil with weak sinking motion in the lowest levels ahead (southeast) of the reflectivity maximum. When the reflectivity maxima moved toward the northeastern portion of the rainband and matured, high reflectivities associated with them was observed southeast of the convergence zone. The westerly inflow from the rear became more significant in the lowest 4-5 km. Downward motion dominated within the reflectivity maxima in the lower troposphere. Rising motion was located northwest of the echo maximum and along the low-level wind-shift line. The reflectivity maxima dissipated on the northeastern end of the rainband as they moved inland. The continuous generation of new reflectivity maxima along the wind-shift line maintained the long lifetime of the rainband, and produced persistent heavy rainfall along the northwestern Taiwan coast as they moved toward the coast. The heaviest rainfall occurred when the wind-shift line arrived in the northwestern coast.

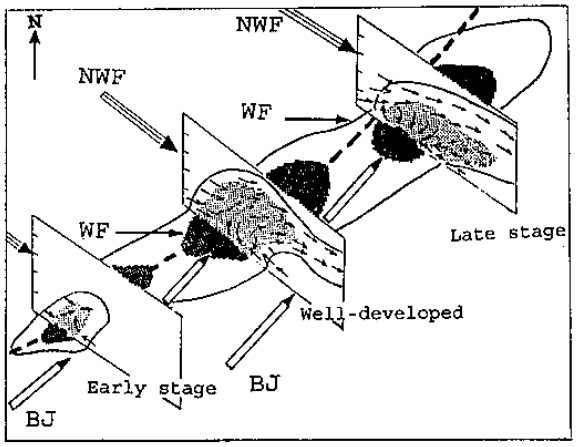

Figure 7 Schematic diagram for the structure of the rainband. The barrier jet (BJ) converges with the westerly flow (WF) along the wind-shift line (heavy, dashed line) in low levels. The northwesterly flow (NWF) dominates in the upper troposphere. The vertical cross sections show the long-lived reflectivity maxima embedded in the rainband at the early, well-developed, and late stage, respectively. The solid lines represent radar echo boundary with reflectivity core areas shaded. The thin arrows on the cross sections indicate the relative airflow to the rainband system.

b. Case of IOP 2

On 17 May, 1987 (IOP 2), the barrier jet was also observed along the northwest coast with much higher daily rainfall along the northwest-to-north coastal regions than along the west-to-southwest coastal regions. Previous studies of IOP 2 (Wang et al., 1990; Lin et al., 1990; Chen, 1991; Tao et al., 1991) were concentrated on the structure and the development of a squall line moved inland along the northwestern coast around 0100 LST. Nevertheless, most of the rainfall over the Taiwan area on 17 May, especially along the northwest-to-north coast, was contributed by a pre-existing convective system over north South China Sea which moved inland just before noon. The

formation and the characteristics of the rainfall system and the mesoscale flow pattern for IOP 2 are different from those in IOP 13. For IOP 13, the interaction between the barrier jet and the westerly flow coming from off the southeastern China coast behind the trough is important for the development and maintenance of a prefrontal rainband (Li et al.,1996). For IOP 2, the low-level flow at the 850-hPa level was northeasterly along the southeastern China coast in the morning hours as the convective system moved northeastward to the western coast of Taiwan. The pre-existing convective system is enhanced in the prefrontal region off the northwestern coast in the convergence zone between the southwest monsoon flow and the southerly barrier jet (not shown). In the postfrontal region, the low-level northerly flow dominated over the southeastern China and the northern Taiwan. The enhancement of the radar echoes was also evident along the frontal boundary

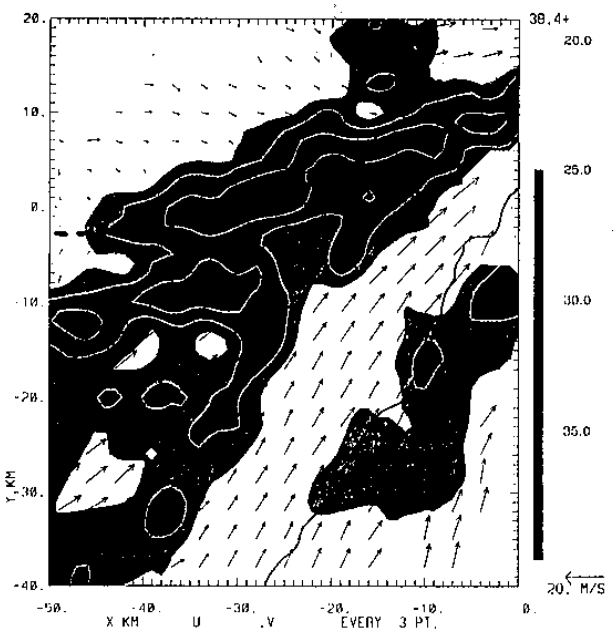

Figure 8 Horizontal winds bu dual Doppler analysis in superimposition with reflectivity contours every 5 dBZ at 1 km around 1008 LST 17 May. Heavy dashed line and thin line represent the location of the surface front and the coastal line of Taiwan.

where the southerly barrier jet converged with the post-frontal northerly flow (Fig. 8). The low-level convergence zone between the barrier jet and the environment flow played an important role in focusing rainfall along the northwestern coast.

6. Summary and discussion

With a steep terrain over Taiwan, the interaction between the low-level southwesterly monsoon flow and the island topography is significant during the early-summer rainy season. In the past decade, the synoptic-scale low-level jet (LLJ) has been extensively studied, but the orographic influence on the flow near and over the island had not been well understood. The barrier jet is a local feature over northwestern Taiwan, and it is different from the well-known low-level jet defined by Chen and Yu (1988). The overall features of the barrier jet and the LLJ are summarized in Table 2. The barrier jet maximum altitude is at ~ 1 km, about 1.2 km lower than the LLJ height. The vertical wind shear is about 10×10^{-3} s^{-1} below the barrier jet level and 4×10^{-3} s^{-1} above, respectively. The shear magnitudes below the barrier jet level is about twice the shear below the LLJ. The barrier jet has a smaller horizontal length scale than the LLJ (Table 2). In addition, the barrier jet is parallel to the central mountain range, whereas the orientation of the LLJ varies from case to case between the north-south to the east-west direction, and depends on the orientation of the large-scale 850-hPa pressure pattern (Chen and Yu 1988; Chen and Chen 1995). The temporal scale of the barrier jet varies from case to case. For the 13 May case, the occurrence of the barrier jet ($V_s \geq 10$ m s^{-1}) was less than 12 h (Fig. 2a). For the 22-25 June case, however, the jet persisted more than 3 days (Fig. 2a). The barrier jet develops as the upstream southwesterly flow intensifies and impinges at the central mountain range. The barrier jet reaches the maximum intensity when the orographic blocking of the southwesterly flow by the island obstacle is most significant. It weakens as a surface front arrives over northwestern Taiwan and dissipates when the surface front are over the island.

A schematic diagram for the jet formation is shown Figure 9. As a large-scale low-pressure system moves eastward toward the eastern China coast, strong southwesterly flow is present ahead of the pressure trough and along the southeastern China coast (Fig. 9a). This is the large-scale background for the development of barrier jet. Over the Taiwan area, a windward ridge develops along the western coast with a pressure trough on the lee under the southwesterly flow regime. The low-level incoming southwesterly flow decelerates off the southwestern coast when it

	Barrier Jet (TAMEX)	Low-Level Jet
Maximum altitude(km)	~ 1.0	~ 2.2
Length (km)	≤ 200	> 600
Offshore width (km)	~ 100	------
Orientation (dir)	Parallel to the NW coast (or CMR)	SW - NE
Vertical wind shear($\times 10^{-3}$ s^{-1}) (below)	~ 10	~ 6
(above)	~ 4	~ 3
Formation mechanism	Interaction between SW flow and the island topography	Large-scale processes

Table 2 Comparison of the features between the barrier jet during TAMEX and the low-level jet (LLJ) defined by Chen and Yu(1988).

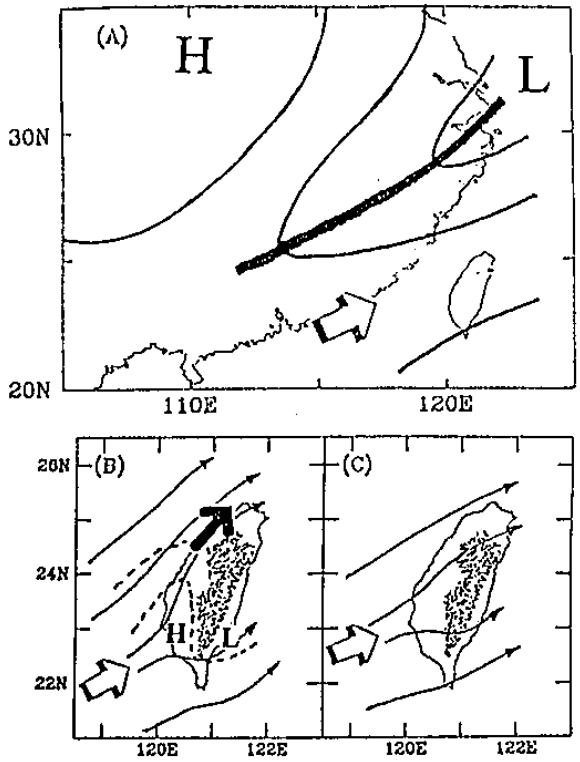

Figure 9 A schematic diagram for the barrier jet formation. The large-scale low-level flow pattern(a), the mesoscale airflow near the 1-km level(b) and at 2.5-km level © over the Taiwan area are shown. The heavy line, open arrow and heavy arrow represent the low-level pressure trough, upstream southwesterly flow and barrier jet, respectively. The distribution for the geopotential height in (a), local sea-level pressure pattern (dashed) in (b) and stream lines (solid) in (b) and (c) are also shown. Terrain contours as in Fig.1.

encounters the high pressure there. The flow splits offshore of the coast and moves around the island (Fig. 9b). Along the western coast, the deflected airflow accelerates northward with a large cross-contour wind component down the pressure gradient along the northwestern coast, resulting in locally strong alongshore winds (the barrier jet) over northwestern Taiwan. Above the average height (~ 2 km) of the central mountain range, the windward pressure ridge is less pronounced and the flow acceleration along the northwestern coast becomes smaller than the lower level. The incoming southwesterly flow is only slightly deflected by the island obstacle and moves over the mountain range (Fig. 9c). As shown in Figure 3b, the depth of the mixing boundary layer is about 1 km for the seven TAMEX barrier jet cases. It is speculated that although the maximum pressure gradients occur at the surface along the northwestern coast, the strong turbulence would reduce the wind speed in the boundary layer. As a result, the flow acceleration becomes smaller at the surface than near the top of the boundary layer. Therefore, the barrier jet occurs at the top (~ 1 km) of the mixing boundary layer along the northwestern coast.

Although this study shows a close relationship between the jet and the intensity of the windward pressure along the western coast, a detailed diagnostics of the force balance from the primitive equation are needed to fully understand the physical processes responsible for the formation of the jet. This requires dense data coverage not only along the shore but also in the direction normal to the shore. A high-resolution mesoscale model will be used to simulate the jet and to assess the physical mechanisms responsible for its formation. In addition, the role of the barrier jet in the enhancement of heavy rainfall over northwestern Taiwan is discussed from two case studies. Additional case studies are needed to understand the role the barrier jet in focusing heavy rainfall along the western/northwestern coast when large-scale conditions are favorable.

Acknowledgments

We would like to thank all participants involved in the planning and the execution of TAMEX. Part of the computing resources is supported by the Scientific Computing Division of the National Center for the Atmospheric Research, which is sponsored by the National Science Foundation. This work is supported by the National Science Foundation under Grant ATM-9421060.

REFERENCES

Bell, G. D., and L. F., Bosart, 1988: Appalachian cold-air damming. Mon. Wea. Rev., 116, 137-161.

Chen, C. -S., 1991: A numerical study of a squall line over the Taiwan Strait during IOP 2. Mon. Wea. Rev., 119, 2677-2698.

Chen, T. G. -J., and C. - C. Yu, 1988: Study of low-level jet and extremely heavy rainfall over northern Taiwan in the Mei-Yu season. Mon. Wea. Rev., 116, 884-891.

Chen, S., and A. Schumann, 1990: Taiwan area mesoscale experiment: Conventional data and user's guide. NCAR Tech. Note, NCAR/TN-349+1A, 123pp.

Chen, X. A., and Y.-L. Chen, 1995: Development of low-level jets during TAMEX. Mon. Wea. Rev., 123. 1695-1719.

Y. -L. Chen, and N. B. - F. Hui, 1990: Analysis of a shallow front during the Taiwan area mesoscale experiment. Mon. Wea. Rev., 118, 2649-2667.

-----, and J. Li, 1995a: Characteristics of surface pressure and wind patterns over the island of Taiwan during TAMEX. Mon. Wea. Rev. 123, 691-716.

-----, and -----, 1995b: Large-scale conditions for the development of heavy precipitation during TAMEX IOP 3. Mon. Wea. Rev., 123, 2978-3002.

Cunning, J. B., 1988: Taiwan area mesoscale experiment: Daily operations summary, NCAR Technical Note NCAR/TN-305+STR,

Doyle, J.D., and T.T. Wanner, 1991: A Carolina coastal low-level jet during GALE IOP 2. Mon. Wea. Rev., 119, 2414-2428.

Kuo, Y. - H. and G. T. - J. Chen, 1990: The Taiwan area mesoscale experiment: An overview. Bull. Amer. Meteor. Soc., 71, 488-503.

Li, J., Y, -L. Chen, and W. -C Lee, 1996: Analysis of a heavy rainfall event during TAMEX. Mon. Wea. Rev., (in press).

Overland, J.E., 1984: Scale analysis of marine winds in Straits and along mountainous coasts. Mon. Wea. Rev., 112, 2530-2534.

-----, and N. A. Bond, 1995: Observations and scale analysis of coastal wind jet. Mon. Wea. Rev., 123, 2934-2941.

Parish, T. R., 1982: Barrier winds along the Sierra Nevada. J. Appl. Meteor., 21, 925-930.

Schwerdtfeger, W., 1975: Mountain barrier effect of the flow of stable air north of the Brooks Range. The 24th Conf. of Climate of the Arctic, Fairbanks, Alaska, 204-208.

Smith, R. B., 1979: The influence of mountains on the atmosphere. Advances in Geophysics, Vol. 31, Academic Press, 1-41..

-----, 1982: Synoptic observations and theory of orographically disturbed wind and pressure. J. Atmos. Sci., 39, 348-364.

-----, 1989: Mountain-induced stagnation points in hydrostatic flow. Tellus, 41A, 270-274.

Smolarkiewicz, P. R., R. M. Rasmussen and T. L., Clack, 1988: On the dynamics of Hawaiian cloud bands: Island forcing. J. Atmos. Sci., 45, 1872-1905.

Stull, R. B., 1988: An introduction to boundary layer meteorology. Kluwer Academic publishers, The Netherlands. 666 pp.

Sun, W. -Y., J. D. Chern, C. -C. Wu, and W. -R. Hsu, 1991: Numerical simulation of mesoscale circulation in Taiwan and surrounding area. Mon. Wea. Rev., 119, 2558-2573.

Tao, W. K., and Simpson J., 1991: Numerical simulation of a subtropical squall line over the Taiwan Strait. Mon. Wea. Rev., 119, 2699-2723.

Wang, S. -T., 1986: Observational analysis of the interaction between fronts and the orography in Taiwan during the late winter monsoon season. International Conf. on Monsoon and Mesoscale Meteor. Nov. 4-7, 1986, Taipei, Taiwan, 123-135.

Wang, T. -C. C., Y. -J. Lin and R. W. Pasken and H. Shen, 1990: Characteristics of a subtropical squall line determined frpm TAMEX dual-Doppler data. Part I: kinematic structure. J. Atmos. Sci., 47, 2357-2381.